Journal of Sound and Vibration (1994) **174**(5), 641–654

FLUID–STRUCTURAL COUPLING OF A PLATE-ENDED CYLINDRICAL SHELL: VIBRATION AND INTERNAL SOUND FIELD

L. CHENG

Department of Mechanical Engineering, Université Laval, Québec, Canada G1K 7P4

(*Received* 7 *July* 1992, *in final form* 8 *March* 1993)

This paper presents a theoretical study of a plate-ended circular cylindrical shell radiating sound into its enclosed cavity. On the basis of a previously established free vibration model, a general formulation considering the full coupling between the subsystems (plate, shell and cavity) is developed. By using an artificial spring system, this formulation allows, in a systematic way, the consideration of a wide variety of boundary conditions and shell–plate joint conditions. Numerical results on the structure vibration and the generated sound field inside the cavity are presented. These results are intended to investigate two main issues: (1) obtaining a deep understanding of the coupling phenomena, which is a key factor to understand the mechanism of the mechanical energy transfer between the plate and the shell and mechanical–acoustical energy transfer from the structure to the acoustic medium; (2) illustrating the possibilities and limitations of sound-proofing by changing shell–plate joint conditions. The established model is believed to be useful in industrial applications where plate-ended shell structures are involved, especially in the case of the modelling of aircraft structures and fluid-containing industrial vessels.

1. INTRODUCTION

In this continuation of the study of the vibroacoustic behavior of a plate-ended cylindrical shell, a previously derived free vibration formulation [1] is extended in this paper to take into account the coupling of the structure with the enclosed acoustic medium. The plate-ended cylindrical shell structure is of particular interest to study for many industrial applications. The most representative examples for this are first, the study of an aircraft fuselage closed by a circular bulkhead in which case the vibration of the structure, as well as the induced cabin noise, is a major concern and, second, industrial vessels for which the contained fluid has a significant influence on the structure.

The work performed in the past on the plate-ended shell has mainly focused on free vibration analyses [1–4]. As far as the fluid–structural coupling analysis is concerned, much less information is available. When validating an analytical model for aircraft interior noise prediction via experiments, Pope *et al.* [5] considered the effects of end caps. In their analysis, the internal pressure due to the end cap motion was estimated in an approximate way, since the plate was supposed to be independent of the fuselage shell. Recently, Bafilios *et al.* [6] presented a plate-ended composite shell model to study the structure-borne noise transmission. In a similar way, no coupling between the shell and the plate was allowed. The shell and the plate were supposed to be simply supported along their edges, and the acoustic pressure inside the enclosure was calculated simply by superposing the contribution of each substructure.

0022-460X/94/300641 + 14 $08.00/0

The present study is an extension of a previous work [1] on a free vibration model in which full coupling between the shell and the plate was considered. That paper predicted the superiority of the proposed method over most existing approaches which treat mechanically coupled structures when one desires to treat further fluid–structure coupling problems. Another advantage of the model was its systematic modelling of various structural coupling cases and boundary conditions by means of an artificial spring system. On the basis of this free-vibration model, further development is carried out in the present paper to include the acoustic medium inside the enclosure. For this purpose, hard-walled cavity modes are used as a basis for the decomposition for sound pressure as well as the Green's function of the cavity. The resulting equations, in which the full interactions (plate–shell and structure–cavity) are taken into account, are then solved. Furthermore, the paper contains numerical results on the vibration of the shell and the end plate and also on the generated sound pressure field in the cylindrical enclosure. Taking advantage of the flexible modelling of the structural coupling, and using the concepts put forward previously concerning the nature of the combined structure modes, coupling analyses are performed.

With respect to existing work in the literature, the present study is believed to contribute in the following aspects: (1) it offers a general formulation in which both plate–shell coupling and structure–fluid coupling are permitted; (2) the formulation encompasses a wide spectrum of boundary conditions and coupling conditions that may be encountered in practice; (3) the performed analysis provides physical insight into the vibroacoustic behavior of the system and reveals possible means for sound-proofing.

2. ANALYTICAL MODEL

2.1. DESCRIPTION OF THE MODEL

Consider a finite circular cylindrical shell closed at its left end ($x = 0$) by a flexible plate and at its right end ($x = L$) by a rigid plate. Both shell and plate are assumed to be thin homogeneous structures. The geometric parameters and the co-ordinate system used in the formulation are defined in Figure 1. The whole structure is assumed to be initially supported by shear diaphragms at each end to which translational and rotational springs, having distributed stiffnesses K_i and C_i ($i = 1, 2, 3$) are added, as illustrated in Figures 1(c) and 1(d). All spring constants are defined in the appropriate units of stiffness per unit length on the contour and are assumed to be constant along the edges. Different boundary conditions and coupling conditions can then be simulated by setting the appropriate spring constants. The excitation is modelled as a harmonic point load at arbitrary locations, situated either on the shell or on the plate.

2.2. STRUCTURAL RESPONSE

The governing equations of the plate-ended shell are obtained by using the variational principle via the finding of the extremum of Hamilton's function over a suitable subspace of displacement trial functions. A detailed treatment on the free vibration of the structure is given in reference [1]. Due to the very lengthy expressions obtained, only an outline is given here, with special attention paid to the excitation terms and structure–cavity coupling terms.

Hamilton's function of the structure is constructed as

$$H = \int_{t_0}^{t_1} (T_c - E_c + T_p - E_p - E_k + E_F)\,\mathrm{d}t, \tag{1}$$

The present study is an extension of a previous work [1] on a free vibration model in which full coupling between the shell and the plate was considered. That paper predicted the superiority of the proposed method over most existing approaches which treat mechanically coupled structures when one desires to treat further fluid–structure coupling problems. Another advantage of the model was its systematic modelling of various structural coupling cases and boundary conditions by means of an artificial spring system. On the basis of this free-vibration model, further development is carried out in the present paper to include the acoustic medium inside the enclosure. For this purpose, hard-walled cavity modes are used as a basis for the decomposition for sound pressure as well as the Green's function of the cavity. The resulting equations, in which the full interactions (plate–shell and structure–cavity) are taken into account, are then solved. Furthermore, the paper contains numerical results on the vibration of the shell and the end plate and also on the generated sound pressure field in the cylindrical enclosure. Taking advantage of the flexible modelling of the structural coupling, and using the concepts put forward previously concerning the nature of the combined structure modes, coupling analyses are performed.

With respect to existing work in the literature, the present study is believed to contribute in the following aspects: (1) it offers a general formulation in which both plate–shell coupling and structure–fluid coupling are permitted; (2) the formulation encompasses a wide spectrum of boundary conditions and coupling conditions that may be encountered in practice; (3) the performed analysis provides physical insight into the vibroacoustic behavior of the system and reveals possible means for sound-proofing.

2. ANALYTICAL MODEL

2.1. DESCRIPTION OF THE MODEL

Consider a finite circular cylindrical shell closed at its left end ($x = 0$) by a flexible plate and at its right end ($x = L$) by a rigid plate. Both shell and plate are assumed to be thin homogeneous structures. The geometric parameters and the co-ordinate system used in the formulation are defined in Figure 1. The whole structure is assumed to be initially supported by shear diaphragms at each end to which translational and rotational springs, having distributed stiffnesses K_i and C_i ($i = 1, 2, 3$) are added, as illustrated in Figures 1(c) and 1(d). All spring constants are defined in the appropriate units of stiffness per unit length on the contour and are assumed to be constant along the edges. Different boundary conditions and coupling conditions can then be simulated by setting the appropriate spring constants. The excitation is modelled as a harmonic point load at arbitrary locations, situated either on the shell or on the plate.

2.2. STRUCTURAL RESPONSE

The governing equations of the plate-ended shell are obtained by using the variational principle via the finding of the extremum of Hamilton's function over a suitable subspace of displacement trial functions. A detailed treatment on the free vibration of the structure is given in reference [1]. Due to the very lengthy expressions obtained, only an outline is given here, with special attention paid to the excitation terms and structure–cavity coupling terms.

Hamilton's function of the structure is constructed as

$$H = \int_{t_0}^{t_1} (T_c - E_c + T_p - E_p - E_k + E_F)\,\mathrm{d}t, \tag{1}$$

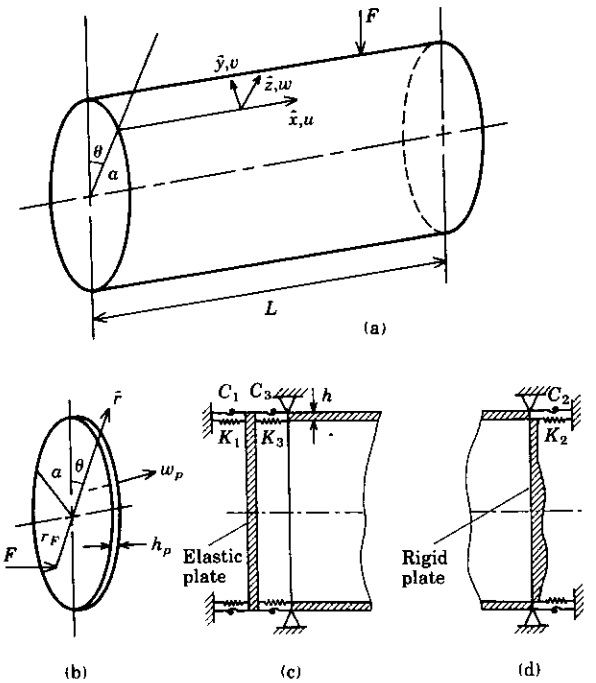

Figure 1. A schematic representation of the plate-ended shell and the co-ordinate system used in the formulation: (a) cylindrical shell; (b) end plate; (c) joint conditions between the shell and the plate at $x = 0$; (d) boundary modelling at $x = L$.

where t_0 and t_1 are arbitrary times, T_c and T_p are, respectively, the kinetic energy of the cylindrical shell and the plate, E_c and E_p are their potential energies, E_k represents the potential energy stored in the springs and E_F is the work done by the driving forces. The calculations of these energy terms can be done by using classical shell and plate theory [7] under appropriate assumptions of structural displacements.

The shell displacements u, v and w along the three axes defined in Figure 1 are then decomposed on the basis of the eigenfunctions of a shear diaphragm supported shell as

$$\begin{Bmatrix} u \\ v \\ w \end{Bmatrix} = \sum_{\alpha=0}^{1} \sum_{n=0}^{\infty} \sum_{m=1}^{\infty} \sum_{j=1}^{3} A^{\alpha}_{nmj}(t) \Pi^{\alpha}_{nmj}(\alpha, n, m, j), \tag{2}$$

where Π^{α}_{nmj} is the eigenvector of the shear diaphragm shell with n and m being, respectively, the circumferential and the longitudinal order, α indicates symmetric ($\alpha = 1$) or antisymmetric ($\alpha = 0$) modes and j is the type of mode (bending, twisting or extension–compression) [8]; the $A^{\alpha}_{nmj}(t)$ are the coefficients to be determined. Since the continuation conditions between the plate and the shell are characterized by the artificial springs between them, Π^{α}_{nmj} only needs to satisfy the geometrical boundary conditions related to the radial and tangential directions ($w = v = 0$), which is the case here.

As for the plate, its flexural displacement w_p is expended over a polynomial basis:

$$w_p = \sum_{\alpha=0}^{1} \sum_{n=0}^{\infty} \sum_{m_p=0}^{\infty} B^{\alpha}_{nm_p}(t) \Lambda^{\alpha}_{nm_p}(\alpha, n, m_p), \qquad \Lambda^{\alpha}_{nm_p}(\alpha, n, m_p) = \sin(n\theta + \alpha\pi/2)(r/a)^{m_p}, \tag{3}$$

where n, m_p and α are, respectively, the circumferential order, the radial order and the symmetric index, a is the radius of the plate and the $B^{\alpha}_{nm_p}(t)$ are the coefficients to be determined.

Using expressions (2) and (3), the Hamilton's function H can be expressed in terms of two sets of unknowns, $A^{\alpha}_{nmj}(t)$ and $B^{\alpha}_{nm_p}(t)$. The extremization of H can then be done by following the Rayleigh–Ritz procedure. Upon assuming the sinusoidal motion

$$A^{\alpha}_{nmj}(t) = A^{\alpha}_{nmj}\exp(\mathrm{j}\omega t), \qquad B^{\alpha}_{nm_p}(t) = B^{\alpha}_{nm_p}\exp(\mathrm{j}\omega t), \tag{4}$$

we obtain the following equations:

$$M_{nmj}(\omega^2_{nmj}(1+\mathrm{j}\eta_c)-\omega^2)A^{\alpha}_{nmj} + \sum_{m'=1}^{\infty}\sum_{j'=1}^{3} X^{\alpha}_{nmjm'j'}A^{\alpha}_{nm'j'} - \sum_{m_p=0}^{\infty} Y^{\alpha}_{nmjm_p}B^{\alpha}_{nm_p},$$

$$= -(F^{\alpha}_{nmj})_{shell} + (P^{\alpha}_{nmj})_{shell}, \tag{5}$$

$$\sum_{m'_p=0}^{\infty}(R^{\alpha}_{nm_pm'_p}(1+\mathrm{j}\eta_p)-\omega^2 M^{\alpha}_{nm_pm'_p})B^{\alpha}_{nm'_p} + \sum_{m'_p=0}^{\infty} Z^{\alpha}_{nm_pm'_p}B^{\alpha}_{nm'_p}$$

$$-\sum_{m=1}^{\infty}\sum_{j=1}^{3} Y^{\alpha}_{nmjm_p}A^{\alpha}_{nmj} = (F^{\alpha}_{nm_p})_{plate} - (P^{\alpha}_{nm_p})_{plate}. \tag{6}$$

In the above expressions, ω_{nmj} and M_{nmj} are, respectively, the natural frequencies and the generalized modal masses of the shear diaphragm supported shell, $R^{\alpha}_{nm_pm'_p}$ and $M^{\alpha}_{nm_pm'_p}$ are the stiffness and mass terms of the plate and, finally, $X^{\alpha}_{nmjm'j'}$, $Y^{\alpha}_{nmjm_p}$ and $Z^{\alpha}_{nm_pm'_p}$ are the coupling terms via different spring systems. Detailed expressions for the calculations of these terms have been given in previous work [1]. Also in the above expressions, the structural damping factors η_c and η_p have been introduced for the shell and the plate respectively. On the right side of the equations, one notices the direct excitation terms $(F^{\alpha}_{nmj})_{shell}$ and $(F^{\alpha}_{nm_p})_{plate}$ and the fluid loading terms from the cavity $(P^{\alpha}_{nmj})_{shell}$ and $(P^{\alpha}_{nm_p})_{plate}$.

2.3. ACOUSTIC RESPONSE

The pressure inside the enclosure P_c satisfies the classical wave equation

$$\nabla^2 P_c + (\omega/c)^2 P_c = 0, \tag{7}$$

with c being the speed of sound in the cavity. The boundary conditions to be satisfied are

$$\partial P_c/\partial r = -\rho\omega^2 w, \quad \text{at } r = a; \qquad \partial P_c/\partial x = \rho\omega^2 w_p, \quad \text{at } x = 0;$$

$$\partial P_c/\partial x = 0, \quad \text{at } x = L. \tag{8}$$

Note that w_p is assumed to be positive along the positive x-axis. By means of the Green's function G of the cavity with Neumann boundary conditions, the sound pressure P_c inside the cavity can be calculated as

$$P_c = -\int_A G(\partial P_c/\partial\tilde{n})\,\mathrm{d}A, \tag{9}$$

where A is the total area of the structure envelope and $\tilde{n}$ is the unit vector normal to the corresponding surface (positive toward the outside). Using equation (8), the above expression becomes

$$P_c = \int_{S_1} G\rho\omega^2 w\,\mathrm{d}S_1 - \int_{S_2} G\rho\omega^2 w_p\,\mathrm{d}S_2, \tag{10}$$

where S_1 and S_2 are, respectively, the shell and plate surface. Both the pressure P_c and the Green's function G are then expanded in terms of the acoustic modes of the hard-walled cavity Φ_N. For P_c, one has

$$P_c = \rho c^2 \sum_{N=1}^{\infty} P_N \Phi_N / M_N, \qquad M_N \delta_{NM} = (1/V) \int_V \Phi_N \Phi_M \, \mathrm{d}V, \tag{11, 12}$$

in which the P_N are the coefficients to be determined, V is the volume occupied by the cavity and δ_{NM} is the Kronecker delta function. The second expression reflects the orthogonality of acoustic modes. For the Green's function G, it can be shown [9] that

$$G(\tilde{M}_v, \tilde{M}_{v'}, \omega) = \sum_{N=1}^{\infty} \frac{c^2}{VM_N} \frac{\Phi_N(\tilde{M}_v)\Phi_N(\tilde{M}_{v'})}{(\omega_N^2 - \omega^2)}, \tag{13}$$

with ω_N being the angular frequency of the Nth cavity mode.

Substituting expressions (11)–(13) into equation (10) yields

$$(\omega_N^2 - \omega^2) P_N = (S/V)\omega^2 w_N, \qquad S = S_1 + S_2, \tag{14}$$

in which

$$w_N = (-1/S) \int_{S_1} w \Phi_N \, \mathrm{d}S_1 + (1/S) \int_{S_2} w_p \Phi_N \, \mathrm{d}S_2. \tag{15}$$

The applications of the expressions (11)–(15) to the case of a cylindrical cavity give equations characterizing the acoustic response. In this case, each mode is represented by four indices: α, n, p and q. Consequently, the mode index N used above will be replaced by the combination of α, n, p and q modal indices. The mode shape and the corresponding angular frequency are

$$\Phi^{\alpha}_{npq} = \sin(n\theta + \alpha\pi/2) \mathrm{J}_n(\lambda_{np} r) \cos[(q\pi/L)x], \qquad \omega_{npq} = c[\lambda_{np}^2 + (q\pi/L)^2]^{1/2}, \tag{16, 17}$$

where α is the symmetric index, n is the circumferential order, J_n is the nth order Bessel function, q is the longitudinal order, and λ_{np} is the pth root of equation

$$\mathrm{J}'_n(\lambda_{np} a) = 0. \tag{18}$$

Considering the displacement decomposition of the structure (expressions (2) and (3)), together with expressions (15) and (16), equation (14) becomes

$$(\omega^2_{npq} + \mathrm{j}\eta_v \omega_{npq} \omega - \omega^2) P^{\alpha}_{npq} = (\omega^2 S/V) \left[\sum_{m=1}^{\infty} \sum_{j=1}^{3} L^{shell}(\alpha, n, q, m) A^{\alpha}_{nmj} - \sum_{m_p=0}^{\infty} L^{plate}(\alpha, n, p, m_p) B^{\alpha}_{nm_p} \right]. \tag{19}$$

In the above expression, the damping in the cavity is expressed in terms of a modal damping factor η_v. $L^{shell}(\alpha, n, q, m)$ and $L^{plate}(\alpha, n, p, m_p)$ are, respectively, the spatial shell–cavity and plate–cavity coupling coefficients defined as follows:

$$L^{shell}(\alpha, n, q, m) = (1/S) \int_{S_1} [\Pi^{\alpha}_{nmj}]_w \Phi^{\alpha}_{npq} \, \mathrm{d}S_1, \qquad L^{plate}(\alpha, n, p, m_p) = (1/S) \int_{S_2} A^{\alpha}_{nm_p} \Phi^{\alpha}_{npq} \, \mathrm{d}S_2, \tag{20}$$

where $[\Pi^{\alpha}_{nmj}]_w$ is the w component of the eigenvector Π^{α}_{nmj}.

Using the spatial coupling coefficients as defined, the excitation terms appearing on the right side of equations (5) and (6) can then be calculated by

$$(F^{\alpha}_{nmj})_{shell} = -\int_{S_1} F\delta(\tilde{M}-\tilde{M}_F)[\Pi^{\alpha}_{nmj}]_w \,\mathrm{d}S_1, \quad \tilde{M}\in S_1;$$

$$(F^{\alpha}_{nmp})_{plate} = \int_{S_2} F\delta(\tilde{M}-\tilde{M}_F)\Lambda^{\alpha}_{nm_p}\,\mathrm{d}S_2, \quad \tilde{M}\in S_2,$$

$$(P^{\alpha}_{nmj})_{shell} = \frac{\rho c^2 S^2\omega^2}{V}\left[\sum_{m'=1}^{\infty}\sum_{j'=1}^{3}\sum_{p=1}^{\infty}\sum_{q=0}^{\infty}\frac{L^{shell}(\alpha,n,q,m)L^{shell}(\alpha,n,q,m')}{(\omega^2_{npq}-\omega^2)M^{\alpha}_{npq}}A^{\alpha}_{nm'j}\right.$$

$$\left.-\sum_{m_p=0}^{\infty}\sum_{p=1}^{\infty}\sum_{q=0}^{\infty}\frac{L^{shell}(\alpha,n,q,m)L^{plate}(\alpha,n,p,m_p)}{(\omega^2_{npq}-\omega^2)M^{\alpha}_{npq}}B^{\alpha}_{nm_p}\right],$$

$$(P^{\alpha}_{nm_p})_{plate} = \frac{\rho c^2 S^2\omega^2}{V}\left[-\sum_{m=1}^{\infty}\sum_{j=1}^{3}\sum_{p=1}^{\infty}\sum_{q=0}^{\infty}\frac{L^{plate}(\alpha,n,p,m_p)L^{shell}(\alpha,n,q,m)}{(\omega^2_{npq}-\omega^2)M^{\alpha}_{npq}}A^{\alpha}_{nmj}\right.$$

$$\left.+\sum_{m'_p=0}^{\infty}\sum_{p=1}^{\infty}\sum_{q=0}^{\infty}\frac{L^{plate}(\alpha,n,p,m_p)L^{plate}(\alpha,n,p,m'_p)}{(\omega^2_{npq}-\omega^2)M^{\alpha}_{npq}}B^{\alpha}_{nm'_p}\right]. \tag{21}$$

In the above expressions, F is the driving point force acting either on the shell or on the plate surface, its direction being illustrated in Figure 1; $\delta(\tilde{M}-\tilde{M}_F)$ is the Kronecker delta describing the driving force applied at the point $\tilde{M}_F$.

In conclusion, equations (5), (6) and (19) constitute a whole coupled equation system, the resolution of which gives the coefficients A^{α}_{nmj} and $B^{\alpha}_{nm_p}$ for the calculation of the structural response and the coefficients P^{α}_{npq} for the determination of the sound pressure in the cavity.

3. NUMERICAL RESULTS

Numerical results are presented herein for the average sound pressure level inside the cavity and for the quadratic velocity of the shell and the end plate. As far as the shell response is concerned, only radial velocity is considered. The quadratic velocity is represented in terms of dB referenced to 5×10^{-8} m/s. The shell and the plate are assumed to have the same material properties as aluminium (Young's modulus 7×10^{10} N/m^2, density $2{\cdot}7\times10^3$ kg/m^3 and Poisson ratio 0·3). The dimensions of the shell are $L = 1{\cdot}2$ m and $a = 0{\cdot}3$ m. The thicknesses of the shell and the end plate are selected to be the same for both and equal to 3 mm. Due to the limitless combinations that can arise regarding the boundary conditions, only a special case is investigated herein with all the spring constants K_i and C_i set to zero except K_3 and C_3, the values of which are defined in each case investigated. This means, physically, that the structure which will be studied is, as a whole, simply supported with adjustable shell–plate joint conditions. For K_3 and C_3, two non-dimensional stiffness parameters are defined with respect to the flexural rigidity of the plate D_p as $\tilde{K} = K_3a^3/D_p$ and $\tilde{C} = C_3a/D_p$. The speed of sound in the interior and the air density are $c = 340$ m/s and $\rho = 1{\cdot}2$ kg/m^3. The input load is a unit point force acting at a certain location of the shell surface or the end-plate surface. In all calculations performed, the modal loss factors for the plate, the shell and the cavity are set to be 0·01. As illustrated in a previous work [10], system damping plays an important part in determining the system response. More specifically, damping values affect the response of the system in a significant way at resonances. Since the present work focuses mainly on the coupling analysis, no details about damping effects are presented hereafter.

The frequency range considered is 0–2000 Hz. The linear system (equations (5), (6) and (19)) should be truncated to a finite order before the execution of the calculations. The truncation of the series is a curtail issue which requires careful consideration. Generally speaking, the criterion for choosing the maximum order of each index appearing in the decomposition series (2), (3) and (11) is to assure the characterization of the coupling and the convergence of the solution. One simplified means of doing this is to increase the terms and to check the modes of each substructure until the natural frequency for each index pair exceeds a limiting frequency. It should be noted that the so-called limiting frequency is usually set to be higher than the frequency of interest which is considered. As a result, not only all within-band modes are considered, but also some out-of-band ones. For the present configuration, the limiting frequency is set to 2300 Hz. For the cavity, based on the aforementioned criterion, an automatic selection procedure is established. In addition to that, for certain values of n, where the natural frequency of even the lowest cavity mode exceeds the upper limit of the considered frequency range, the first nine lowest modes are also taken into consideration.

Convergence was carefully checked by increasing the number for each variable involved in the expansion series. As far as the structural response is concerned, relatively good convergence was noticed. The reason is believed to be twofold: for the shell, a "physical" base is used, which is by nature quite similar to the real structure (as far as the shell portion is concerned); for the plate, the boundary is uniform and homogeneous, although the expansion series is less "physical". Irregularities presented in the structures may be a key factor to slow down the convergence of the Rayleigh–Ritz procedure [11]. In our case, the shell–plate connection is uniform and symmetric, so that no such strong variation was present. As to the cavity response, the solution converged even more rapidly than the structural response. In this paper, all the calculations were done by using 15 terms for n, 11 for m_p and 20 for m. With this truncation procedure, 1800 component modes were used for the shell, 330 for the plate and 338 for the cavity. Thanks to the non-coupling property between the components with different circumferential orders, the calculation were performed with a reasonable cost and a satisfactory accuracy.

It has been shown [1] that the mechanical properties of the shell–plate combined structures are closely related to the characteristics of each substructure. A good knowledge on the natural frequencies of the substructures gives a basic idea of the nature of the generated modes for the combined structure. More precisely, it has been shown that three types of modes exist for the combined structure. The first two types are shell-controlled and plate-controlled modes, for which the structure motion is dominated, respectively, by shell and plate vibrations. This situation happens when the mechanical impedances of the uncoupled structures are quite different, corresponding to the case in which the natural frequencies of the uncoupled substructures of the same circumferential order are not close enough to form a structure mode. The third type of modes are coupled modes, with the shell and the plate vibrating in the same order of magnitude. This phenomenon occurs when there exists a mechanical impedance adaptation of the substructures. In addition to the structure modes, the distribution of the cavity modes is another crucial factor affecting the acoustic response. A lattice diagram describing the modal distribution of the three subsystems constituting the system (plate, shell and cavity) is presented in Figure 2. The calculations are performed with the subsystems assumed to be uncoupled from each other. The shell is assumed to be supported by shear diagrams at both ends, the plate simply supported along its edge and the cavity having acoustically hard walls. In the diagram, the calculated modes are arranged in columns by regrouping the modes having the same circumferential order and are represented by using different symbols. In fact, the diagram reflects the dispersion relation of different waves in each subsystem and is very revealing

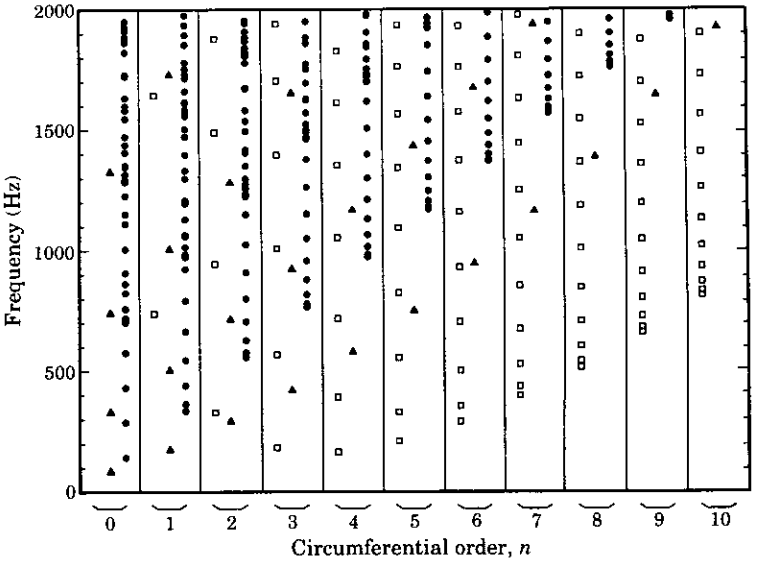

Figure 2. A lattice diagram of the structural modes and the acoustic modes: □, shell modes; ▲, plate modes; ●, cavity modes.

in the interpretation of the physical phenomena that will be observed. One important point to mention comes from the observation of the coupling equations (5), (6) and (19): the shell–plate coupling, as well as the structure–cavity coupling, occurs in a very selective manner. In fact, only the terms having the same circumferential order (the modes arranged in the same column in Figure 2) can possibly be spatially coupled.

The average quadratic velocities of the structure and the corresponding sound pressure level inside the cavity are presented in Figures 3 and 4 respectively. In the calculations, the plate is assumed to be rigidly attached to the shell, with $\hat{K}_3 = \hat{C}_3 = 10^8$. A unit point load is applied on the shell surface at $x = 0{\cdot}35$ m, and all damping values are set to be 0·01. In Figure 3, the response of the shell and the plate are, respectively, illustrated by the solid and the dashed line. In the response of the shell, one can clearly identify the presence of

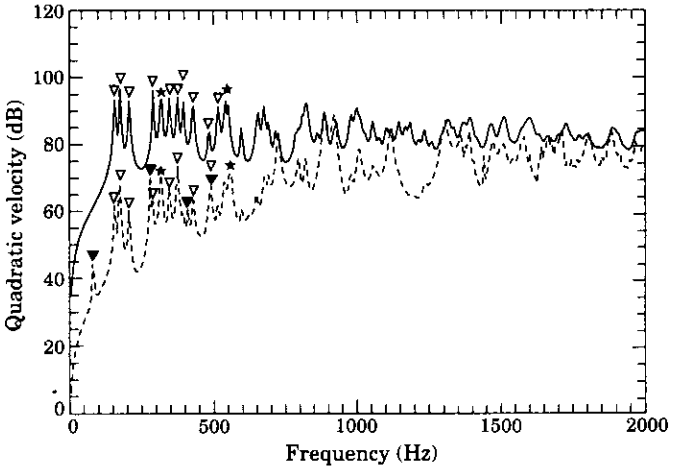

Figure 3. The quadratic velocity of the structure with the shell subjected to a unit point load: ——, shell; – – –, plate; ▽, shell-controlled mode; ▼, plate-controlled mode; ★, coupled mode.

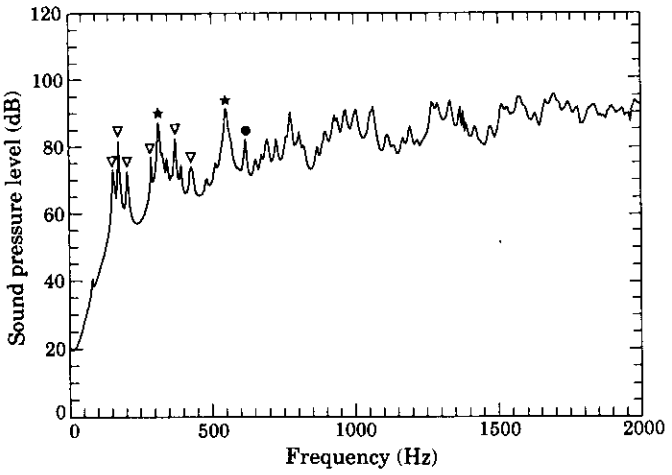

Figure 4. The average sound pressure level inside the cavity generated by the structure motion with the shell subjected to a unit point load: ▽, shell-controlled mode; ★, coupled mode.; ●, cavity mode.

shell-controlled modes and some coupled modes. However, no plate-controlled modes are noticeable in this shell response spectrum. It is in the spectrum of the plate that the plate-controlled modes, together with shell-controlled and coupled modes, appear. The results of Figure 3 indicate that the coupling between the shell and the plate is relatively weak in the low frequency range. In fact, the vibration level of the shell, which is the element directly excited by the external loads, is much higher than the one of the plate. With the increase of the frequency, the velocity of the plate is brought up to a comparable level. The corresponding sound pressure level inside the cavity is presented in Figure 4. It can be seen from this figure that the noise level takes an ascending trend with frequency. Two obvious reasons explain these observations. Firstly, the motion of the shell contributes nearly all acoustic energy in the lower frequency region. In fact, the sound pressure is totally dominated by shell-controlled and coupled modes and, as mentioned above, the response of the plate is much lower than the one of the shell in this frequency range. Secondly, the shell has weak radiation capacity at lower frequencies. The fact that few acoustic modes emerge below 1000 Hz indicates that the shell modes are poorly coupled to the acoustic ones. Indeed, a review of Figure 2 shows that the natural frequencies of the acoustic modes increase monotonously with their circumferential order. Consequently, only those with small circumferential order can contribute significantly to the sound field in the low frequency range. However, the excited shell modes in this frequency range are not necessarily of small circumferential order. For example, the shell modes with $n = 0$ are situated near the ring frequency of the shell which, in the present case, is about 2830 Hz. As already stressed, the structure is only capable of coupling the acoustic modes having the same circumferential order. Therefore, the shell-controlled modes that contribute significantly to the structural response cannot excite efficiently the acoustic modes that would have been the main contributors of sound.

In Figures 5 and 6, the same structural configuration is used, but the point load is located on the surface of the end plate at $r = 0{\cdot}2$ m. Several similar observations made previously apply to the present case. Being directly excited, the plate manifests a dominating role in the structural response. The plate velocity is clearly dominated by plate-controlled and coupled modes. With respect to the plate motion, the shell vibrates at a level that is about 30 dB lower at low frequencies and 5–10 dB lower at higher frequencies (up to 2000 Hz). However, in terms of sound pressure level in the cavity (Figure 6), many more cavity modes

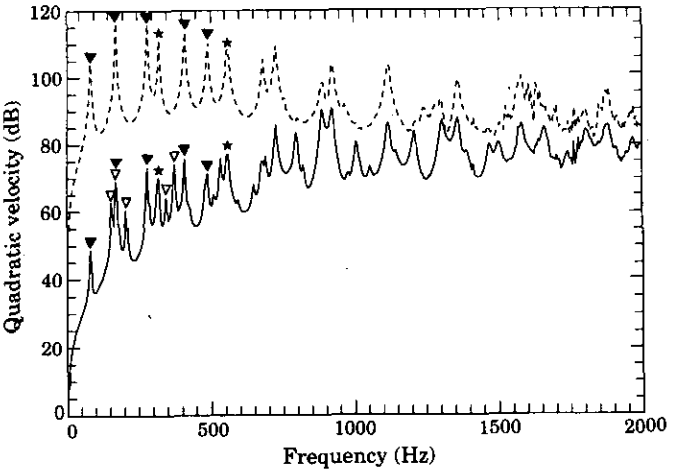

Figure 5. The quadratic velocity of the structure with the end plate subjected to a unit point load: ——, shell; – – –, plate; ▽, shell-controlled mode; ▼, plate-controlled mode; ★, coupled mode.

are excited. This is also understandable due to the fact that plate modes evolve almost in the same way as the acoustic modes with the increase of the circumferential order (Figure 2). Therefore, better coupling between the plate and the cavity is obtained. For the same reason, and also because of the relatively weak rigidity of the plate at low frequencies, the sound pressure level inside the cavity is much higher when it is the plate that is directly excited. In fact, a comparison between Figures 4 and 6 indicates a difference of about 20 dB below 800 Hz. This observation shows the importance of the identification of the excitation sources for such a structure and that it is preferable to guide excitations to the shell rather than to the end plate.

Numerical results that will be presented hereafter aim to illustrate the effects of the joint conditions between the shell and the plate on the generated cavity noise. As has been pointed out, by setting different values for the two spring stiffness constants K_3 and C_3, which can vary from zero to infinity, both limit cases (free or rigid joint) and intermediate cases can be simulated. Despite this possibility offered by the model, only a few limit cases

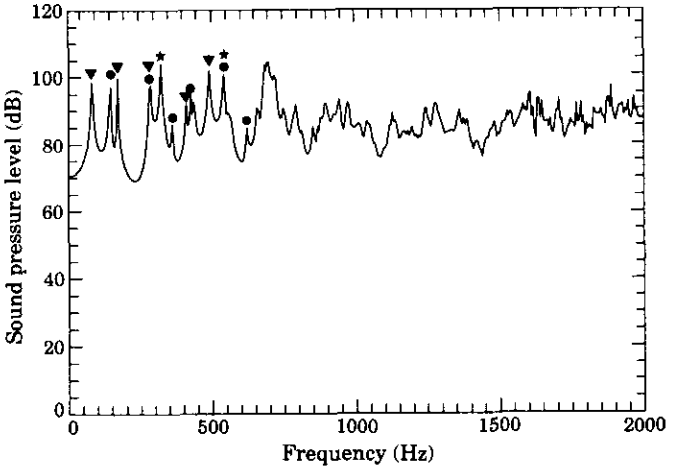

Figure 6. The average sound pressure level inside the cavity generated by the structure motion with the end plate subjected to a unit point load: ▼, plate-controlled mode; ★, coupled mode; ●, cavity mode.

are treated with the stiffness constants set to either zero or a large value. Although zero stiffness is only an idealized assumption that may be hardly encountered in practical circumstances, it is believed that the study of these limit cases is representative and gives upper and lower bound of the observed phenomena for other intermediate joint cases.

The first series of results deal with the effects of the translational spring K_3, which couples the plate with the shell in the longitudinal axis of the latter. In order to isolate the effects of K_3, the value of the rotational spring C_3 is assumed to be zero, permitting no possible coupling via rotation. The same point load as has been used before is applied to the surface of the plate. In Figure 7(a) sound pressure levels inside the cavity are compared with two different joint conditions: $\hat{K}_3 = 10^8$ (rigid case) and $\hat{K}_3 = 0$. It can be seen that, except at very low frequencies, the structure without translational coupling ($\hat{K} = 0$) radiates much less sound in a very large frequency range. An average of the sound level in one-third octave bands permits a better visualization of the global trend (Figure 7(b)). In fact, a difference of 10–15 dB in sound level is clearly observed for middle and high frequency bands. This observation is consistent with the one made in a previous work [12], where the sound radiation to a cylindrical hard-walled cavity by a single plate with various boundary conditions was investigated. Similar phenomena were observed in that work regarding the translational support of the plate. Moreover, a detailed analysis

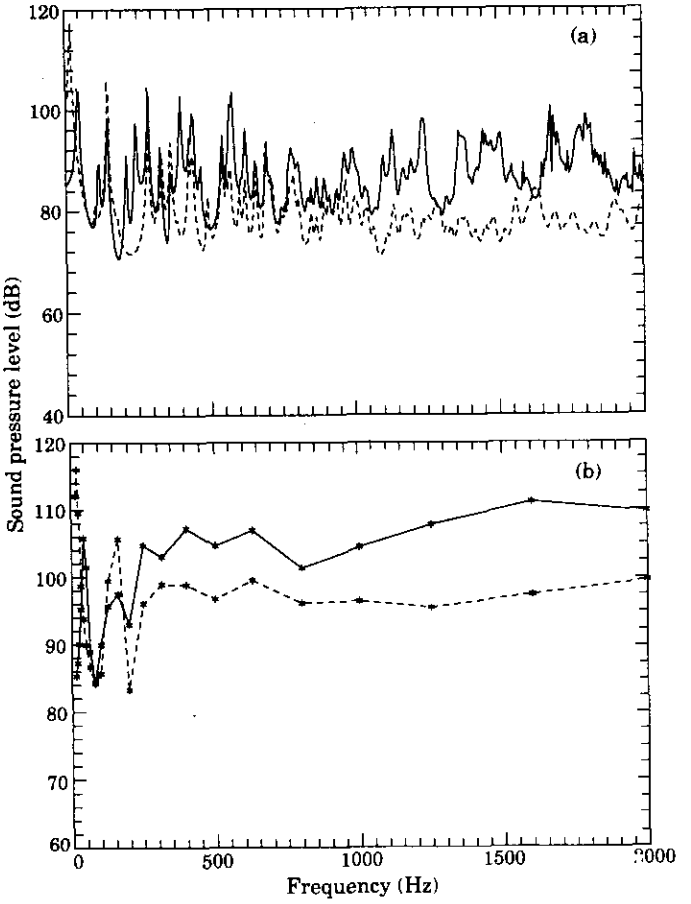

Figure 7. The average sound pressure level inside the cavity with two limiting shell–plate joint conditions in translation. (a) Narrow bands: ——, $\hat{K}_3 = 10^8$; – – –, $\hat{K}_3 = 0$. (b) One-third octave bands: —*—*—*—*—, $\hat{K}_3 = 10^8$; —*—*—*—*—, $\hat{K}_3 = 0$.

showed that releasing the translational support of the plate reduces significantly the radiation efficiency of the plate modes and consequently, the generated noise. In Figures 7(a) and (b) it is shown that the cylindrical wall as a flexural envelope does not change this trend fundamentally. In addition to that, the diminution of K_3 reduces the plate–shell coupling via translation, so that the contribution of the shell radiation, although small in the present case, is also reduced.

The second series of results concern the effects of the rotational spring C_3, coupling the plate with the shell via the rotation along the edge. The internal noise level is presented in Figures 8(a) and (b), in narrow bands and one-third octave bands, respectively. Two values for C_3 are chosen for the calculations: $\hat{C}_3 = 10^8$ (rigid joint) and $\hat{C}_3 = 0$. From Figures 8(a) and (b), a less noticeable reduction than the one previously made for K_3 is obtained by relaxing the rotational coupling. Although small perturbations are noticed at low frequencies, the noise inside the cavity is not very sensitive to the coupling changes in this range. All the principal peaks appearing in the spectrum in this frequency range are governed by cavity resonances. For frequencies higher than 1000 Hz, the noise level is reduced to a lower level by reducing the rotational coupling. However, with a hard-walled cylindrical cavity [12], no such trend was observed when reducing the rotational fixation of the end plate, and it was shown that the radiation properties of the plate cannot be improved systematically by changing the rotational supports (which is the case for translational ones!). It is therefore concluded that the noise reduction obtained in the present case is due to the fact that, by relaxing the rotational coupling, the vibration level of the shell is reduced and, consequently, its sound radiation. This statement is

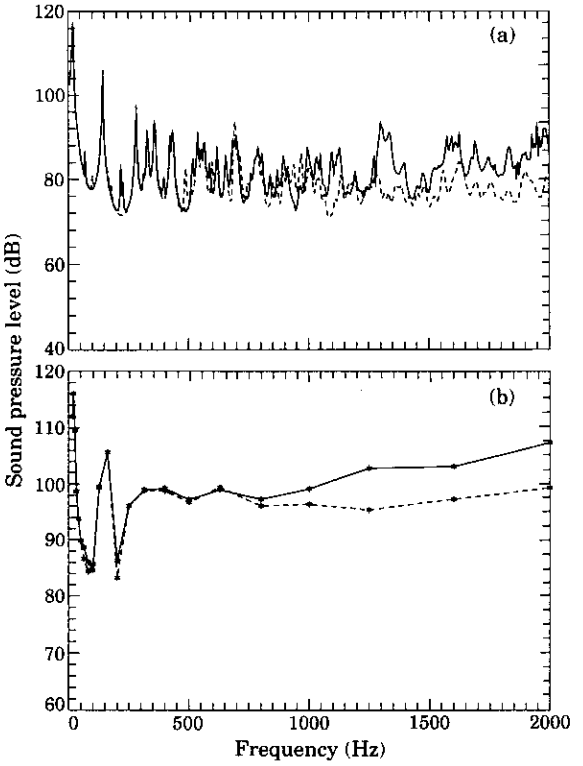

Figure 8. The average sound pressure level inside the cavity with two limiting shell–plate joint conditions in rotation. (a) Narrow bands: ——, $\hat{C}_3 = 10^8$; – – –, $\hat{C}_3 = 0$. (b) One-third octave bands: —*—*—*—*—, $\hat{C}_3 = 10^8$; —*—*—*—*—, $\hat{C}_3 = 0$.

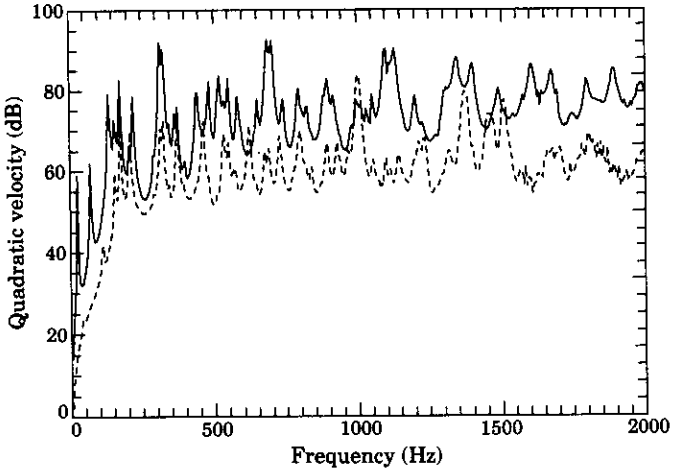

Figure 9. The quadratic velocity of the shell excited by the end plate via coupling in rotation (solid line) and in translation (dashed line): ——, $\hat{C}_3 = 10^8$; – – –, $\hat{K}_3 = 10^8$.

supported by Figure 9, in which the velocity spectrum of a shell excited only by rotational coupling ($\hat{C}_3 = 10^8$) is compared with the one excited only by translational coupling ($\hat{K}_3 = 10^8$). Keeping in mind that the point load is applied to the end plate surface, one notices a clear difference between the two curves, indicating that the shell is coupled to the plate mainly through rotation.

Similar investigations have been performed when excitation loads are applied on the shell surface. However, it has been observed that the changes of the coupling conditions in this case cannot give any general trends, as is the case with excitations on the plate.

4. CONCLUSIONS

A general vibroacoustic formulation is developed in this paper for a plate-ended cylindrical shell with consideration of the enclosed acoustic cavity. The model takes into account the full coupling between plate and shell as well as the coupling of the whole mechanical envelope with the acoustic medium. The modeling of boundary conditions and shell–plate joint conditions are made possible by using an artificial spring system working on translation and rotation that allows an easy simulation of a large variety of coupling cases. With point excitation loads on the plate or on the shell, numerical results for the structural response and the cavity noise are presented and analyzed to reveal the general vibroacoustic behavior of the system. The main findings are summarized as follows.

(1) The coupling between the shell and the plate is generally weak at low frequencies. The vibration response of the substructure that is directly excited is dominated by the modes controlled by itself and by coupled modes. Modes of all nature (plate-controlled, shell-controlled and coupled modes) appear generally in the response spectrum of the substructure that is not directly excited. The shell–plate coupling becomes more noticeable with increase of frequency.

(2) Cavity noise comes mainly from the directly excited substructure at low frequencies. The sound pressure level inside the cavity is much higher when excitations are applied to the end plate. The reason is that the plate modes couple generally well with the cavity modes, whereas the shell modes, participating actively in the structure response, cannot

be efficiently coupled to the acoustic ones in this frequency range. Consequently, from a sound-proofing point of view, direct excitations on the plate should be avoided.

(3) For the case in which the excitation is applied to the shell, changing joint conditions cannot warrant any systematic improvement on the radiated sound field inside the cavity. For the case in which the end plate is directly excited, reducing the stiffness of the joint between the shell and the plate proves to be a good means of reducing cavity noise. Two different mechanisms are involved: the diminution of the translational coupling (along the longitudinal axis of the shell) significantly reduces the radiation efficiency of the plate modes, and the diminution of the rotational coupling (coupling created by rotation along the joint) reduces the mechanical energy transferred to the shell. In both cases, cavity noise is reduced. However, the relaxing of the translational coupling seems to give a better result: a greater noise reduction in a broader frequency band.

It should be mentioned that these observations are directly related to the hypotheses made in the modelling process concerning the perfect geometry of the structure. The symmetric properties of the structure, with respect to the shell longitudinal axis, give rise to the selective manner in which the coupling process happens. In reality, the presence of any asymmetric elements may change the coupling nature between the substructures and, consequently, amplify to a certain extent the radiation capacity of the cylindrical shell. This point should be further analyzed.

ACKNOWLEDGMENT

This work was supported by grant OGPIN-013 from the Natural Sciences and Engineering Research Council of Canada (NSERC).

REFERENCES

1. L. CHENG and J. NICOLAS 1992 *Journal of Sound and Vibration* **155**, 231–247. Free vibration analysis of a cylindrical shell – circular plate system with general coupling and various boundary conditions.
2. M. S. TAVAKOLI and R. SINGH 1990 *Journal of Sound and Vibration* **136**, 141–145. Modal analysis of a hermetic can.
3. G. YAMADA, T. IRIE and T. TAMIYA 1986 *Journal of Sound and Vibration* **108**, 297–304. Free vibration of a circular cylindrical double-shell system closed by end plates.
4. K. SUZUKI, S. TAKAHASHI, E. ANZAI and T. KOSAWADA 1983 *Bulletin of the Japan Society of Mechanical Engineers* **26**, 1775–1782. Vibrations of a cylindrical shell with variable thickness capped by a circular plate.
5. L. D. POPE and D. C. RENNISON 1982 *Journal of Sound and Vibration* **84**, 541–575. Development and validation of preliminary analytical models for aircraft interior noise prediction.
6. D. A. BAFILIOS and C. S. LYRINTZIS 1991 *American Institute of Aeronautics and Astronautics Journal* **29**, 1193–1201. Structure-borne noise transmission into cylindrical enclosures of finite extent.
7. W. SOEDEL 1981 *Vibrations of shells and plates*. New York: Marcel Dekker.
8. A. W. LEISSA 1973 *Vibrations of Shells*. NASA SP-288, Washington, D.C.
9. P. M. MORSE and K. U. INGARD 1968 *Theoretical Acoustics*. New York: McGraw–Hill.
10. L. CHENG and C. LESUEUR 1989 *Journal d'Acoustique* **2**, 347–355. Influence des amortissements sur la réponse vibroacoustique. Etude théorique et expérimentale d'une plaque excitée mécaniquement et couplée à une cavité.
11. C. PIERRE, D. M. TANG and E. H. DOWELL 1987 *American Institute of Aeronautics and Astronautics Journal* **25**, 1249–1257. Localized vibrations of disordered multispan beam: theory and experiment.
12. L. CHENG and J. NICOLAS 1992 *Journal of the Acoustical Society of America* **91**, 1504–1513. Radiation of sound into a cylindrical enclosure from a point-driven end plate with general boundary conditions.